Available online at www.sciencedirect.com
ScienceDirect
Acta Materialia 57 (2009) 3402–3409
Acta MATERIALIA
www.elsevier.com/locate/actamat

Development of Al_2O_3–TiO_2 composite ceramics for high-power millimeter-wave applications

T. Kolodiazhnyi [a,*], G. Annino [b], M. Spreitzer [c], T. Taniguchi [a], R. Freer [d], F. Azough [d], A. Panariello [e], W. Fitzpatrick [e]

[a] National Institute for Materials Science, 1-1 Namiki, Tsukuba, Ibaraki 305-0044, Japan
[b] Istituto per i Processi Chimico-Fisici, CNR, Pisa 56124, Italy
[c] Jožef Stefan Institute, Jamova 39, 1000 Ljubljana, Slovenia
[d] Materials Science Centre, School of Materials, University of Manchester, Grosvenor Street, Manchester M1 7HS, UK
[e] Corporate R&D Center, COMDEV International, Cambridge, Ont., Canada N1R 7H6

Received 4 February 2009; received in revised form 12 March 2009; accepted 23 March 2009
Available online 3 May 2009

Abstract

Al_2O_3–TiO_2 composite dielectric ceramics have been prepared by different sintering techniques including high-temperature, high-pressure sintering (2.5 GPa, $T = 1000$ °C) and conventional pressureless sintering ($T = 1350$ °C). Formation of the Al_2TiO_5 secondary phase has been completely suppressed by optimization of the sintering and annealing temperatures. Dielectric properties were measured in the 10–11 GHz range using the cylindrical resonant cavity technique and in the 40–92 GHz range using the open resonator whispering gallery mode technique. At 10 GHz, the optimized composite material (0.895 Al_2O_3–0.105 TiO_2) exhibited $Q \times f = 210$ THz, $\varepsilon' = 12.5$ and $\tau_f = +2.0$ ppm K^{-1} at room temperature. As an evidence of an additional, low-frequency (possibly Debye-type), extrinsic contribution to the dielectric loss, the $Q \times f$ value gradually increased with frequency and reached a plateau of $Q \times f \approx 340$ THz at approximately 80 GHz. It is demonstrated that Al_2O_3–TiO_2 composites have considerable potential as dielectric resonators in the output multiplexers of communication satellites.

Keywords: Dielectric resonator; Dielectric loss; Composite ceramics; Microwaves

1. Introduction

Dielectric resonators based on $Ba(Mg_{1/3}Ta_{2/3})O_3$ (BMT) ceramic are widely used in the input multiplexers of communication satellites operating at low microwave (MW) power. Utilization of this ceramic brings significant reduction in the weight and size of the satellite payload, thus dramatically decreasing the cost and environmental impact of the satellite launch. Unfortunately, due to the low thermal conductivity (i.e. $\kappa \approx 4$ W m^{-1} K^{-1} at 300 K) and strong increase in dielectric loss with temperature, BMT is of limited use in the output multiplexers, which operate at high MW power (e.g. 150–250 W per channel) and over a wide temperature range (−30 to +110 °C).

Alumina with its exceptionally low dielectric loss ($\tan\delta \leqslant 2 \times 10^{-5}$ at 10 GHz) and high thermal conductivity ($\kappa \approx 30$ W m^{-1} K^{-1} at 300 K) is an attractive candidate for dielectric resonator (DR) materials for high-power applications in the MW and particularly the millimeter-wave regions of the electromagnetic spectrum. Another significant advantage of Al_2O_3 is its relatively low cost compared to that of tantalum-based DRs. Unfortunately, alumina has a fundamental drawback. Its dielectric constant increases with temperature, yielding a large negative temperature coefficient of the resonant frequency, τ_f (–60 ppm K^{-1} at 300 K). A possible solution to this limitation is to combine alumina

* Corresponding author. Tel.: +81 29 860 4407; fax: +81 29 860 4706.
E-mail address: kolodiazhnyi.taras@nims.go.jp (T. Kolodiazhnyi).

1359-6454/$36.00 © 2009 Acta Materialia Inc. Published by Elsevier Ltd. All rights reserved.
doi:10.1016/j.actamat.2009.03.050

with another material having a temperature coefficient of resonant frequency of the opposite polarity and acceptable dielectric losses.

Titania with $\tau_f = +450$ ppm K^{-1} appears as an attractive candidate to achieve zero τ_f of a ceramic mixture of Al_2O_3 and TiO_2. Alford's group [1,2] previously reported the doping of alumina with small amounts of TiO_2 and found that this successfully reduced the dielectric loss. But these experiments were not aimed at producing a zero τ_f ceramic. At the same time it was pointed out that tuning of τ_f to 0 ppm K^{-1} might be challenging due to the formation of the Al_2 TiO_5 secondary phase having $\tau_f \approx -90$ ppm K^{-1} [1]. In a later experiment Alford et al. [3] prepared a layered DR structure having $Q = 30{,}000$ at 10 GHz ($Q = 1/\tan\delta$) where a thin TiO_2 layer was"doctor-bladed" on top of a sintered alumina puck. Although the τ_f of this layered DR structure is 0 ppm K^{-1} in the 290–310 K interval, the τ_f was found to be strongly nonlinear outside this temperature range. In addition, layered composite DRs are not practical from a fabrication perspective and, due to the layered design, they are very difficult to tune to a specific resonance frequency without altering the τ_f value. Owing to these drawbacks, more recent efforts have been focused on the optimization of the dielectric properties of bulk Al_2O_3–TiO_2 composite ceramics. Ohishi et al. [4] found that a post-sintering anneal of Al_2O_3–TiO_2 ceramics at 1000 °C is beneficial for removal of the Al_2TiO_5 secondary phase which is thermodynamically unstable below 1180 °C. Kono and co-workers [5] used small additions of MnO to suppress the formation of Al_2TiO_5 during sintering of the Al_2O_3–TiO_2 ceramics at 1350 °C.

Although the Al_2TiO_5 secondary phase can be completely suppressed by a suitable choice of preparation conditions, the finite solubility of Al ions in TiO_2 and Ti ions in the Al_2O_3 host contributes to extrinsic dielectric loss in this composite. Slepetys et al. [8] reported a solubility of 1.5 mol.% for Al_2O_3 in rutile at 1425 °C. Synchrotron X-ray diffraction and Fourier transform infrared spectroscope (FTIR) were employed by Gesenhues and Rentschler [9] to study the defect structures of 0.0–0.8% Al-doped rutile prepared at 930–980 °C. The authors found at least two types of defect equilibria with (i) Al on a substitutional site Al'_{Ti} compensated by an oxygen vacancy $V_O^{\bullet\bullet}$, and (ii) at higher doping levels, Al on a substitutional site, Al'_{Ti}, compensated by Al on an interstitial site, $Al_i^{\bullet\bullet\bullet}$. At even higher doping levels the authors observed clustering of Al^{3+} in the form of $\{ Al'_{Ti} \cdot Al_i^{\bullet\bullet\bullet} \cdot V_O^{\bullet\bullet} \}$ or $\{ Al'_{Ti} \cdot Al_i^{\bullet\bullet\bullet} \}$ (using the conventional Kröger–Vink notation) [9].

The solubility of Ti ions in Al_2O_3 is somewhat lower than that of the Al ions in the TiO_2 host. Nevertheless the solubility of the Ti^{4+} in alumina can reach 0.4 at.% at 1300 °C [10]. According to the high-temperature electrical conductivity measurements of Mohapatra et al. [11], performed under different oxygen partial pressures, Ti^{4+} is substituted for Al^{3+}, forming a positively charged $Ti_{Al}^{\bullet}$ defect. The charge compensation in this case is realized by negatively charged Al vacancies (i.e. V_{Al}'''). These findings have been supported by the subsequent first-principles study of Matsunaga et al. [12]. It is expected therefore that the interaction of these charged defects and dipolar defect complexes with an electromagnetic field would bring additional (i.e. extrinsic) dielectric loss in the Al_2O_3–TiO_2 system.

Taking into account the complexity of the defect chemistry and thermodynamics of the Al_2O_3–TiO_2 system, this paper reports progress and further understanding of this low-loss composite dielectric ceramic.

2. Experiment

Composite dielectric ceramics were prepared from fine Al_2O_3 and TiO_2 powders of 99.99% purity obtained from Alfa Aesar. A number of samples were prepared with small additions of MnO of up to 0.2 wt.%. The powders were wet mixed in Nalgen bottles with ethanol and Tosoh zirconia balls for 20 h. After drying, a small amount of polyvinyl alcohol binder was added and the powders were twice screened through a nylon sieve to ensure a homogeneous distribution of the binder. Green pellets of 10 mm diameter and 4 mm height were uniaxially pressed under a load of 30 MPa. Tungsten carbide pressing dies were used to avoid contamination. The pellets were fired in air at 1300–1350 °C for 5–100 h, then cooled down to 1000 °C and annealed for times in the range 0–200 h. In a separate series of experiments, selected samples were sintered at 1000 °C and a pressure of 2.5 GPa in a belt-type high-pressure apparatus for 5 min (to prevent formation of the Al_2TiO_5 secondary phase above 1180 °C). Phase analysis was undertaken with a Rigaku Ultima III X-ray diffractometer ($\lambda = 0.15406$ nm). Microstructural analysis was performed by scanning electron microscopy (SEM) with a JEOL JSM 5800 microscope equipped with an energy-dispersive X-ray spectrometer (EDS, Oxford-Link Isis 300).

For the TEM analysis, specimens were first ground on 1200 grade SiC to reduce the thickness to approximately 300 μm. They were ultrasonically cut into 3 mm diameter discs (Model KT150, Kerry Ultrasonic Ltd.) then dimpled (Model D500, VCR Group, San Francisco, CA) to reduce the ceramic disc thickness to 30 μm. Finally the discs were ion beam thinned (using a Gatan precision ion polishing system model 691 operating at 4–6 kV). TEM analysis was carried out using a Philips CM200 transmission electron microscope (fitted with an EDAX DX4 EDS system) operating at 200 kV and a Tecnai G2 field emission gun transmission electron microscope (operating at 300 kV) fitted with a high-angular annular dark-field (HAADF) STEM detector. The latter microscope was equipped with a Gatan imaging filter system (GIF), and an EDAX EDS system for microanalysis. HAADF-STEM/EDS analysis was performed to define the compositions of the constituent phases.

Dielectric properties (ε', $\tan\delta, \tau_f$) at 10–11 GHz were determined with an Agilent E8364B vector network analyzer. The dielectric resonator was centered on a quartz

support inside a silver-clad cylindrical resonant cavity utilizing $TE_{01\delta}$ resonance mode. The dielectric constant and unloaded Q-factor ($Q \approx 1/\tan\delta$) of the DR were obtained using QWED software which takes into account both the geometry of the DR and the resonant cavity as well as the thermal expansion and conduction loss of the cavity [13]. The temperature dependence of the resonant frequency and the Q-factor were measured in the range 20–110 °C with temperature uncertainty of ±1 K. For dielectric characterization at higher frequencies, e.g. 40–92 GHz, we employed the open resonator whispering gallery mode (WGM) technique using an ABmillimetre vector network analyzer [6,7]. In the WGM technique, a DR puck of 8 mm diameter and 0.9 mm thickness was coupled to a tapered dielectric waveguide made of fused quartz in the so-called reaction configuration. The WGM measurements were performed at room temperature.

3. Results and discussion

3.1. Phase composition and microstructure

In agreement with the earlier investigations we detected large amounts of Al_2TiO_5 secondary phase in the Al_2O_3–TiO_2 composite ceramics sintered above 1250 °C. In contrast, sintering at 1000 °C and a pressure of 2.5 GPa yielded dense composite ceramics that were free of the Al_2TiO_5 phase. However, the dielectric properties of the Al_2O_3–TiO_2 composite obtained by the high-pressure sintering were quite poor (e.g. $Q = 4000$ at 11 GHz). Therefore, our subsequent efforts were focused on the optimization of the pressureless sintering of the Al_2O_3–TiO_2 composites.

Fig. 1 shows the XRD patterns of the 0.88 Al_2O_3–0.12 TiO_2 composite ceramics sintered at 1350 °C for 5 h. Ceramics that underwent fast cooling show a significant amount of the Al_2TiO_5 phase. In contrast, the secondary phase is below the XRD detection limit for ceramics subjected to a post-sinter anneal at 1000 °C for at least 5 h. Annealing at 1000 °C for longer times does not cause any noticeable change in the diffraction patterns, yet it significantly affects the dielectric properties, especially the Q-factor and τ_f. In particular, we found that extending the anneal to more than 30 h caused a decrease in the Q-factor, whereas τ_f continued to change towards more positive values. SEM analysis of the Al_2O_3–TiO_2 composites showed that the microstructure contained two phases. Their compositions were determined using EDS; after prolonged annealing the phases correspond to Al_2O_3 and TiO_2. However, for samples subjected to short anneals the individual inclusions were too small for accurate EDS analysis. These results confirm our XRD analysis that the Al_2TiO_5 phase is not present in the microstructure of samples annealed for extended times. Typical microstructures for the samples are shown in Figs. 2 and 3; these correspond to 0.905 Al_2O_3–0.095 TiO_2 composites fired under

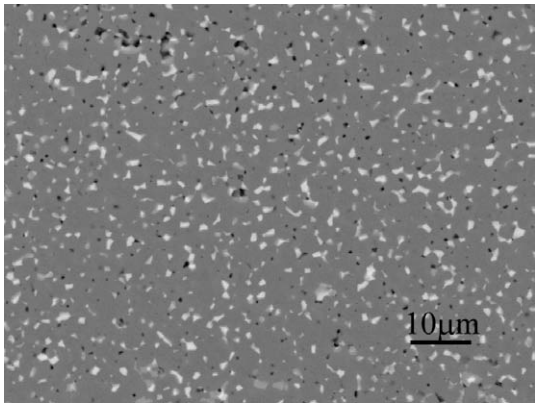

Fig. 2. SEM image of the 0.905 Al_2O_3–0.095 TiO_2 composite sintered at 1350 °C for 5 h and annealed at 1000 °C for 5 h. The light and dark grey areas correspond to TiO_2 and Al_2O_3, respectively.

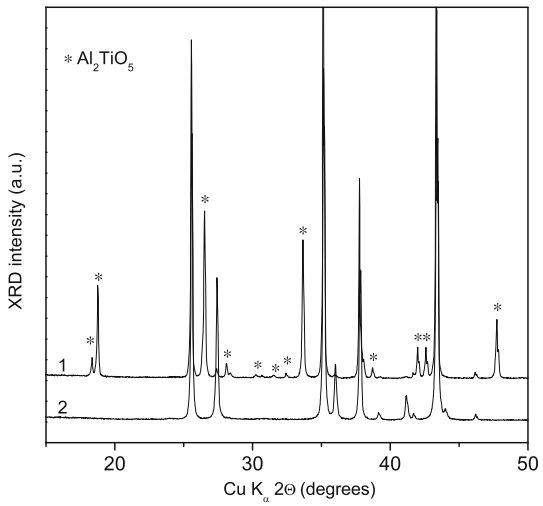

Fig. 1. XRD patterns for the 0.88 Al_2O_3–0.12 TiO_2 composite sintered at 1350 °C and annealed at 1000 °C for 0 h (1) and 200 h (2).

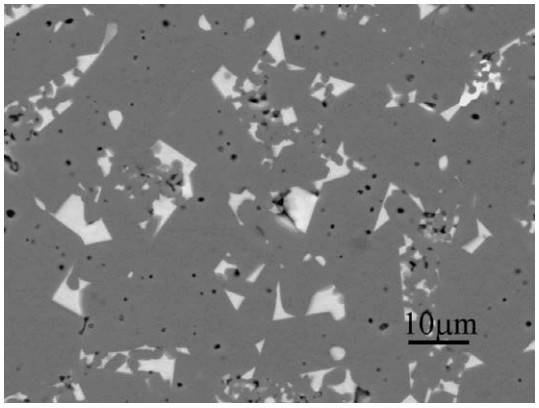

Fig. 3. SEM image of the 0.905 Al_2O_3–0.095 TiO_2 composite sintered at 1300 °C for 100 h and annealed at 1000 °C for 200 h. The light and dark grey areas correspond to TiO_2 and Al_2O_3, respectively.

different conditions. SEM analysis also revealed that the TiO_2 grains are relatively isotropic, homogeneously distributed in the Al_2O_3 matrix and have a narrow size distribution, especially in samples annealed for short times. Moreover, after prolonged annealing, the size of both Al_2O_3 and TiO_2 grains had increased (Fig. 3).

The main purpose of the TEM investigation was to identify the presence of the Al_2TiO_5 phase in the samples. Fig. 4 is a TEM image of sample 0.9 Al_2O_3–0.1 TiO_2 sintered for 5 h at 1350 °C without an anneal. Consistent with XRD analysis of unannealed samples, TEM showed that the sample contains the Al_2TiO_5 phase (arrowed in Fig. 4). In HAADF-STEM (*Z*-contrast imaging), phase identification is usually straightforward since the phases with higher than average atomic number, *Z*, always possess a higher intensity compared to the phases with lower average atomic number, *Z*. Fig. 5 is HAADF-STEM image of sample 0.9 Al_2O_3–0.1 TiO_2 sintered at 1350 °C for 5 h without anneal. The Al_2TiO_5 phase shows medium contrast compared to Al_2O_3 and TiO_2. EDS analysis confirmed the presence of Al_2TiO_5 phase in this sample.

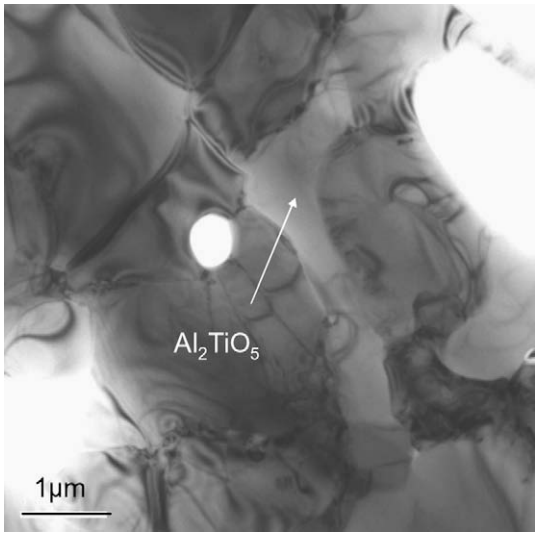

Fig. 4. TEM image of sample 0.9 Al_2O_3–0.1 TiO_2 sintered at 1350 °C without anneal. The arrow indicates the Al_2TiO_5 phase.

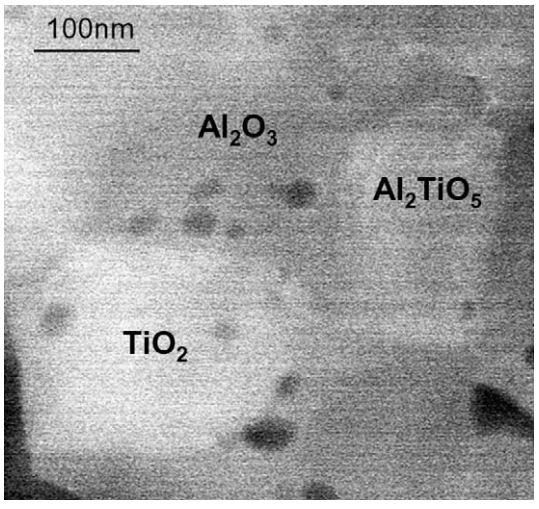

Fig. 5. HAADF-STEM image of sample 0.9 Al_2O_3–0.1 TiO_2 sintered at 1350 °C without anneal.

In agreement with the XRD data and the information from MW property measurements, the microstructure of sample 0.9 Al_2O_3–0.1 TiO_2 (doped with 0.1 wt.% MnO) comprised Al_2O_3 and TiO_2. There was no evidence of the presence of the Al_2TiO_5 phase in this sample. Fig. 6 shows a typical TEM image of sample 0.9 Al_2O_3–0.1 TiO_2 (doped with 0.1 wt.% MnO) sintered at 1350 °C for 5 h and annealed at 1000 °C for 1 h.

3.2. Dielectric properties in the X-band

The TiO_2 doping dependence of the dielectric constant measured at approximately 11 GHz is shown in Fig. 7. The error margins associated with the dielectric constant values are smaller than the area of the datum points in the figure. The dielectric constants of the Al_2O_3–TiO_2 composites have been fitted to the Bruggeman–Polder–van Santen formula. Following the approach proposed by Jylhä [14], the effective dielectric constant, ε'_{eff}, of the composite at a low volume mixing ratio is given by

$$\varepsilon_{eff} = \varepsilon_e + \frac{f}{3}(\varepsilon_i - \varepsilon_e)\sum_{j=x,y,z}\frac{\varepsilon_{eff}}{\varepsilon_{eff} + N_j(\varepsilon_i - \varepsilon_{eff})}, \quad (1)$$

where f is the volume filling fraction, $\varepsilon_e = 9.78$ is the dielectric constant of Al_2O_3, $\varepsilon_i = 100$ is the dielectric constant of TiO_2, and N_j denotes the depolarization factor. For spherical TiO_2 inclusions the depolarization factors are $N_x = N_y = N_z = 1/3$.

In the application of Eq. (1), the isotropic dielectric constant of polycrystalline TiO_2 was employed. It was

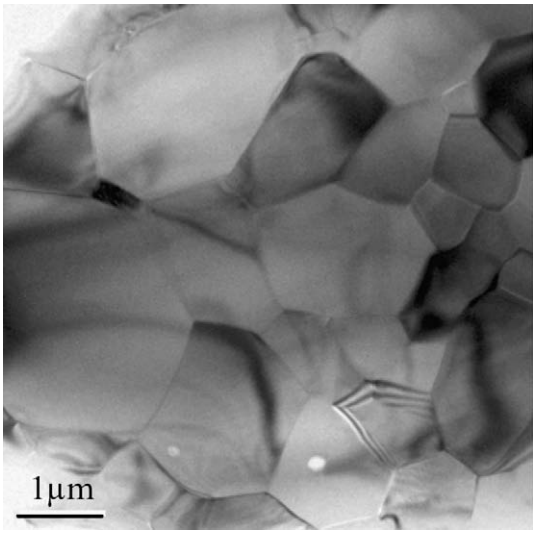

Fig. 6. Typical TEM image of sample 0.9 Al_2O_3–0.1 TiO_2 sample doped with 0.1 wt.% MnO sintered at 1350 °C for 5 h and annealed at 1000 °C for 1 h.

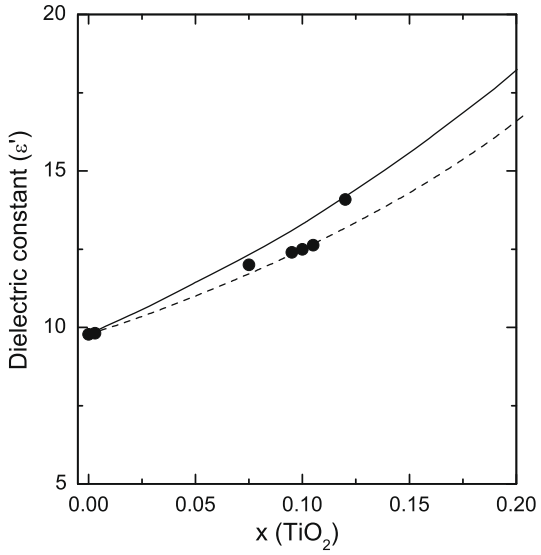

Fig. 7. Dependence of the dielectric constant (ε') on TiO_2 doping for the $(1-x)\,Al_2O_3 - xTiO_2$ composites. The lines are calculated on the basis of the Bruggeman–Polder–van Santen formula, assuming that the TiO_2 inclusions are (i) spheres (dashed line) and (ii) prolate spheroids with semi-axis $a_z = 4, a_x = a_y = 1$ (solid line).

assumed that the TiO_2 behaves as polycrystalline inclusions in the Al_2O_3 matrix. The dashed line in Fig. 7 represents the calculated dependence of the ε_{eff} of the $(1-x)\,Al_2O_3 - xTiO_2$ composite assuming spherical TiO_2 inclusions; it shows fairly good agreement with the experimental data. However, in practice the shape of inclusions may deviate from the ideal spherical form. This could have a noticeable effect on the ε_{eff} even at the low filling limit. As an example, we have also calculated the ε_{eff} assuming that the shape of the TiO_2 particles is close to that of the prolate spheroids with $a_z = 4$ and $a_x = a_y = 1$, where the a_i are the semi-axes. As demonstrated by the solid line in Fig. 7 the effect of TiO_2 inclusions with the shape of prolate spheroids will be to increase the value of the ε_{eff} in the low filling region.

Tuning the temperature coefficient of resonant frequency of the Al_2O_3–TiO_2 composite can be a challenging task. The τ_f exhibits a strong nonlinear dependence on the TiO_2 content, the post-sinter anneal time and the MnO concentration. For example, Fig. 8 shows the effect of MnO doping on τ_f for three different $(1-x)Al_2O_3 - x\,TiO_2$ composites with $x = 0.075$, 0.105 and 0.120. The major source of error in this figure comes from the uncertainty in the MnO concentration due to a small dopant concentration level. Doping the 0.88 Al_2O_3–0.12 TiO_2 composite with 0.1 wt.% of MnO changes the τ_f from -22 to $+30$ ppm K^{-1}. In addition, the τ_f itself shows a nonlinear temperature dependence. This latter dependence is due to the nonlinear temperature dependencies (τ_f) of the individual Al_2O_3 and TiO_2 components of the composite. As reported by Alford et al. [3], the τ_f of Al_2O_3 decreased (nonlinearly) from -33 to -60 ppm K^{-1} in the 180–325 K temperature interval. In the same temperature interval the τ_f of TiO_2 decreased (nonlinearly) from $+690$ to $+420$ ppm K^{-1}. The overall effect is that the τ_f of

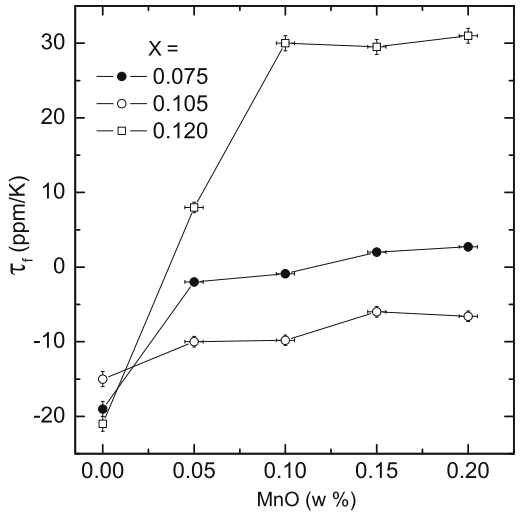

Fig. 8. Effect of the MnO concentration on the τ_f of the $(1-x)\,Al_2O_3 - xTiO_2$ composites sintered at 1350 °C for 5 h. and annealed at 1000 °C for 1 h.

the Al_2O_3–TiO_2 composite DR will have a turning point where its value will change from positive to negative with increasing temperature. This effect is demonstrated in Fig. 9 for a composite DR of 0.895 Al_2O_3–0.105 TiO_2. As evidenced from Fig. 9, the overall drift of the resonance frequency of the 0.895 Al_2O_3–0.105 TiO_2 composite DR does not exceed 2.5 MHz over the temperature interval of 100°C. This behavior is satisfactory for most commercial applications, although the temperature nonlinearity of τ_f vs. T is significant.

MW dielectric loss data for the Al_2O_3–TiO_2 composites, as a function of the TiO_2 content, are summarized in Fig. 10. As expected, the Q-factor decreases when the fraction of the (more lossy) TiO_2 phase is increased. Quantitatively, our data are in good agreement with that of Kono et al. [5]. We confirm that the $Q \times f$ value of Al_2O_3–TiO_2

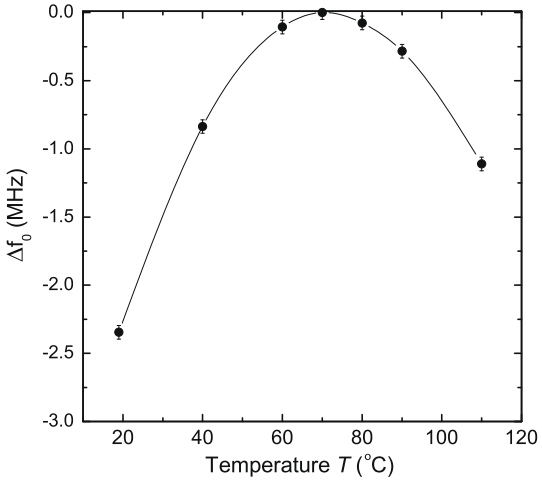

Fig. 9. Temperature dependence of the drift of the resonant frequency of the 0.895 Al_2O_3–0.105 TiO_2 composite DR with a τ_f turning point of 70 °C. The resonance frequency was approximately 10.61 GHz at 70 °C. The line is provided in the figure as a visual guide.

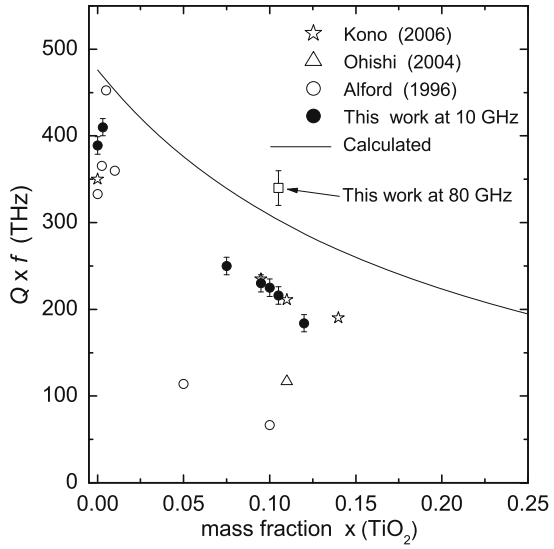

Fig. 10. $Q \times f$ value measured at approximately 10 GHz for the $(1-x)Al_2O_3 - xTiO_2$ (here x is a mass fraction of TiO_2). The graph also includes literature data on MW properties of $(1-x)Al_2O_3 - xTiO_2$ reported by other groups. Solid line is the calculated behavior of the $Q \times f$ estimated using Eq. (3) with $\tan\delta_{Al_2O_3} \approx 2.1 \times 10^{-5}$ and $\tan\delta_{TiO_2} \approx 2 \times 10^{-4}$ at 10 GHz.

composite DRs can be significantly improved by a suitable post-sintering anneal and small additions of MnO. All composite ceramics prepared in this work and reported in Fig. 10 have been sintered at 1350 °C with the exception of pure Al_2O_3 which was sintered at 1600 °C. Remarkably, the 0.997 Al_2O_3–0.003 TiO_2 ceramics sintered at temperatures as low as 1350 °C for 5 h have shown very low dielectric loss ($Q \times f \approx 410$ THz). This sintering temperature is significantly lower than 1600 °C which is usually required to achieve dense Al_2O_3 ceramics with ultra-low dielectric loss [1].

According to Alford et al. [3], for a given electromagnetic mode the dielectric loss, $\tan\delta$, of the Al_2O_3–TiO_2 composite depends on the $\tan\delta$ of the Al_2O_3 and TiO_2 end members and electric filling factors, η, of the TiO_2 inclusions and the Al_2O_3 host, where:

$$\eta_{TiO_2} = \frac{\int_{TiO_2} \varepsilon' < E^2 > dV}{\int_{space} \varepsilon' < E^2 > dV},$$
$$\eta_{Al_2O_3} = \frac{\int_{Al_2O_3} \varepsilon' < E^2 > dV}{\int_{space} \varepsilon' < E^2 > dV}. \quad (2)$$

Here, the brackets indicate the average over the period of the oscillating radiation. Assuming that a negligible fraction of the electric energy of the mode is distributed outside the Al_2O_3–TiO_2 composite, the $\tan\delta$ can be expressed as:

$$\tan\delta = \tan\delta_{TiO_2}\left(1 + \frac{\int_{Al_2O_3} \varepsilon' < E^2 > dV}{\int_{TiO_2} \varepsilon' < E^2 > dV}\right)^{-1} + \tan\delta_{Al_2O_3}\left(1 + \frac{\int_{TiO_2} \varepsilon' < E^2 > dV}{\int_{Al_2O_3} \varepsilon' < E^2 > dV}\right)^{-1} \quad (3)$$

Eq. (3) shows that only the ratio between the integrals of the electric energy over the two components of the medium needs to be calculated.

Accurate determination of the electric filling factors η_{TiO_2} and $\eta_{Al_2O_3}$ requires a volume integration of the electric-field energy stored within the TiO_2 inclusions and Al_2O_3 matrix, respectively. For a random distribution of TiO_2 particles (of random shape) in the Al_2O_3 matrix, this would require extremely intensive computation. To simplify our task we first assumed that the TiO_2 inclusions have a spherical shape and that the diameter of the inclusions is much smaller than the wavelength of the electromagnetic field. In this case we can reduce the problem to finding the electric field E_i inside the spherical particle with dielectric constant ε_i placed in the medium ε_e ($\varepsilon_i > \varepsilon_e$) and exposed to a uniform electric field E_0. This problem has been solved analytically [15]. The constant electric field inside the TiO_2 spherical inclusion is given by:

$$E_i = \frac{3}{\varepsilon_i/\varepsilon_e + 2} E_0. \quad (4)$$

Finally, we assumed that the electric field E_0 inside the Al_2O_3 matrix remains constant and is not significantly altered by the polarization charges at the surface of the TiO_2 spheres. This assumption should hold well for a small volume fraction of TiO_2 inclusions. For a higher volume fraction, one would need a more accurate model which would account for the spatial dependence of the electric field in the Al_2O_3 host. The $Q \times f$ of the Al_2O_3–TiO_2 composite, calculated according to this model by using the relevant data at 10 GHz, is shown as the solid line in Fig. 10. Providing that the above model is still accurate at x (TiO_2) $\leqslant 0.15$, it is evident that the experimental dielectric loss in the optimized composite DRs is significantly higher than that predicted by the model (see Fig. 10). This result suggests the existence of additional (extrinsic) losses in the composite material investigated.

3.3. WGM spectroscopy

Recently, Kono et al. [5] reported an unusual frequency dependence of the 0.9 Al_2O_3–0.1 TiO_2 composite DR whose $Q \times f$ value increased from 211 THz at 12 GHz to 274 THz at 76 GHz. This anomalous behavior of the $Q \times f$ value may indicate an effect of the low-frequency extrinsic dielectric loss (possibly Debye-type loss) whose contribution to $Q \times f$, relative to that of the intrinsic losses, diminishes at higher frequencies. We have examined the frequency dependence of our composite DRs and found qualitatively similar behavior for the $Q \times f$ values. Fig. 11 shows the frequency dependence of the $Q \times f$ value of the 0.895 Al_2O_3–0.105 TiO_2 composite DR measured by the open resonator WGM technique in the 40–90 GHz range. Due to the nature of the WGM technique the low-frequency part of the WGM spectra (in this case the data below 60 GHz) is dominated by radiation losses and should be ignored. The data above 60 GHz are representative of

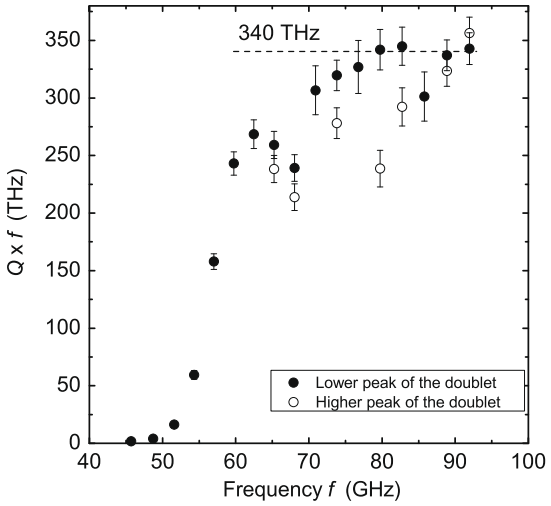

Fig. 11. $Q \times f$ value extracted from the WGM data on the 0.895 Al_2O_3–0.105 TiO_2 composite DR. Above 80 GHz the $Q \times f$ levels off at about 340 THz. Remarkably, at 10 GHz this DR has $Q \times f$ as low as 210 THz.

the true dielectric loss of the composite. Another characteristic of the WGM technique is the occurrence of split resonance modes in inhomogeneous materials. Instead of single peaks, in such materials the resonances can appear as doublets whose components exhibit different quality factors. The doublets arise from a superposition of the two counter-propagating modes associated with a WGM resonance [16]. The different quality factors are related to the different electric field distributions of the components of the doublet, which therefore probe in a different way the (inhomogeneous) material. As a consequence, one of the two modes is more sensitive to the extrinsic losses of the material. Fig. 11 shows the $Q \times f$ obtained for the different resonances; the pair of values corresponding to the same frequency refer to split resonances. The error bars differ for each datum point in Fig. 11. This is due to the effect of the different degree of the splitting of the doublet resonances which affects the accuracy of the determination of the Q-factor. In general, accuracy improves at higher frequencies where splitting of the doublets increases. It can be seen that at 60 GHz the DR shows a $Q \times f$ value of 260 THz. The $Q \times f$ continues to increase with frequency; however, above 80 GHz it reaches a plateau at approximately 340 THz in both components of the doublets. It is remarkable that in the low-frequency region (i.e. 10 GHz) the $Q \times f$ falls to as little as 210 THz.

Within the context of the current theory of intrinsic dielectric loss, we would expect for Al_2O_3 and TiO_2 a linear frequency dependence of $\tan\delta$ in the MW and millimeter-wave ranges, i.e. far below the phonon eigenfrequencies [17]. In contrast, our data confirm that there exists an additional extrinsic contribution to the dielectric loss which causes a significant departure from the linear $\tan\delta \propto f$ behavior at low frequencies. It appears that this extrinsic contribution dominates at lower frequencies as the $\tan\delta \propto f$ relation seems to be recovered above 80 GHz. It is of interest that several other types of dielectric ceramics and single crystals show similar characteristic extrinsic contributions to the dielectric loss at low-frequency (and also at low temperature). For example, a sub-linear $\tan\delta \propto f$ dependence below 60–70 GHz was observed in the $Ba(Mg_{1/3}Ta_{2/3})O_3$, $Ba(Mg_{1/3}Nb_{2/3})O_3$ and $Ba(Co_{1/3}Nb_{2/3})O_3$ ceramics, [7] and a Debye-type dielectric loss with a maximum at 40 K was reported by Shimada et al. for $Ba(Mg_{1/3}\ Ta_{2/3})O_3$ [18]. In another example, a strong low-temperature deviation from intrinsic-type dielectric loss was reported by Aupi et al. for a high-quality alumina [19].

In conclusion, we report the preparation and MW and millimeter-wave dielectric properties of Al_2O_3–TiO_2 composite ceramics, which at 10 GHz exhibit $Q \times f = 210$ THz, $\varepsilon' = 12.5$ and $\tau_f = +2.0$ ppm K^{-1}. It was found that at the MW frequencies the dielectric loss of these materials are dominated by extrinsic sources, possibly associated with point defect complexes due to the finite solubility of Al in TiO_2 and Ti in Al_2O_3. Owing to the relatively slow frequency response of the electromagnetic losses of these defects, the $\tan\delta \propto f$ dependence recovers above 80 GHz. At frequencies above 80 GHz, an optimized Al_2O_3–TiO_2 composite shows high $Q \times f$ value of the order of 340 THz which is close to that predicted in Fig. 10 on the basis of a simple model of spherical TiO_2 inclusions. It is demonstrated that Al_2O_3–TiO_2 composites have considerable potential as dielectric material that can replace the vacuum-filled metal cavities used in the output multiplexers of communication satellites.

Acknowledgements

The authors are grateful to Prof. A. Tagantsev, Dr. Ming Yu and Prof. Le-Wei Li for enlightening discussions. T.K. would like to thank Prof. Jun Akedo for making available the vector network analyzer. This work was supported by MEXT (Japan) and European Space Agency.

References

[1] Alford NMcN, Penn SJ. J Appl Phys 1996;80: 5895.
[2] Breeze JD, Aupi X, Alford NMcN. Appl Phys Lett 2002;81: 5021.
[3] Alford NMcN, Breeze J, Penn SJ, Poole M. IEE Proc-Sci Measure Technol 2000;147: 269.
[4] Ohishi Y, Miyauchi Y, Ohsato H, Kakimoto K. Jpn J Appl Phys 2004;43: L749.
[5] Kono M, Takagi H, Tatekawa T, Tamura H. J Eur Ceram Soc 2006;26: 1909.
[6] Annino G, Bertolini D, Cassettari M, Fittipaldi M, Longo I, Martinelli M. J Chem Phys 2000;112: 2308.
[7] Kolodiazhnyi T, Annino G, Shimada T. Appl Phys Lett 2005;87: 212908.
[8] Slepetys RA, Vaughan PA. J Phys Chem 1969;73: 2157.
[9] Gesenhues U, Rentschler T. J Solid State Chem 1999;143: 210.
[10] Powers JD. Ph.D. Dissertation, University of California, Berkely; 1997.
[11] Mohapatra SK, Kröger FA. J Am Ceram Soc 1977;60: 381.
[12] Matsunaga K, Nakamura A, Yamamoto T, Ikuhara Y. Phys Rev B 2003;68: 214102.

[13] <www.qwed.eu>.
[14] Jylhä L, Sihvola A. J Phys D: Appl Phys 2007;40: 4966.
[15] Jackson JD. Classical electrodynamics. 3rd ed. John Willey; 1998. p. 158–9.
[16] Annino G, Kolodiazhnyi T, Martinelli M. In: Sixth international symposium on physics and engineering of microwaves, millimeter and submillimeter waves (MSMW'07) and workshop on Terahertz technology (Teratech'07), Kharkov, Ukraine, vol. 1; 2007. p. 109–14.
[17] Gurevich VL, Tagantsev AK. Adv Phys 1991;40: 719.
[18] Shimada T, Ichikawa K, Minemura T, Kolodiazhnyi T, Breeze J, Alford N McN, Annino G, submitted for publication.
[19] Aupi X, Breeze J, Ljepojevic N, Dunne LJ, Malde N, Axelsson A-K, et al. J Appl Phys 2004;95: 2639.